



## Review on corrosion-wear resistance performance of materials in molten aluminum and its alloys

Xian-man ZHANG, Wei-ping CHEN

Guangdong Key Laboratory for Advanced Metallic Materials Processing, South China University of Technology, Guangzhou 510640, China

Received 5 August 2014; accepted 28 December 2014

**Abstract:** The failure caused by the corrosion-wear of molten aluminum and its alloys is one of the main problems in aluminum industry. In this work, the resistance behavior of various materials, including Fe-based alloys, ceramics and corresponding high apparatus of corrosion-wear in molten aluminum and its alloys, were reviewed. The synergistic effect of corrosion and wear was discussed based on corrosion and wear mechanics. The effects of dynamic agitation due to rotating of friction pairs, physical property of liquid metal and size of grain etc., on the corrosion-wear resistance performance were investigated. In addition, the characteristics of corrosion-wear resistance performance of materials in molten aluminum and its alloy were summarized. According to our recent progress referred to kinds of materials, especially a  $\text{TiAl}_3/\text{Ti}_3\text{AlC}_2/\text{Al}_2\text{O}_3$  composite, the ceramics/metal composites with a co-continuous structure will be of great advantage in the field of corrosion-wear environment of molten aluminum and its alloys.

**Key words:** molten aluminum; aluminum alloy; corrosion; wear; synergistic effect; intermetallics

### 1 Introduction

Corrosion-wear is one of the extreme states present in engineering process. Different from corrosion-wear in aqueous media which have been found primarily based on an electro-chemical process, the corrosion-wear in molten metal involves not only the corrosion caused by the high temperature molten metal, but also the synergistic effect between corrosion and wear, which results in much greater material losses than the simple sum of losses by either process alone. It is in fact a kind of mechanical–physical–chemical process that involves dissolution, diffusion, reactions in solid and liquid, wear and interaction among them. The changes in microstructure, surface morphology, and composition of the interface between solid and liquid during this process degrade the physical and mechanical properties of the structure materials sharply [1–6]. Molten aluminum and its alloys are one of the most aggressive metal melts due to their high chemical activity with nearly all metals and metal oxides [7–9]. Therefore, the solid contamination and system failure resulting from corrosion-wear of molten aluminum are unavoidable in the aluminum

industry, such as the crucible and die casting mould.

Recently, corrosion by molten aluminum and its alloys [10], and corrosion-wear in aqueous media have been investigated widely [11]. However, there are less reports focused on the corrosion-wear caused by molten aluminum and its alloys. It is therefore highly desirable to learn more about it in order to explore new material that with high corrosion and wear resistance in future. Since there have been no standardized test apparatus and theory until now, this paper will introduce some test apparatus firstly, and then explain corresponding corrosion-wear properties in molten aluminum and its alloys. Various alloy materials, especially Fe-based metals, are summarized, and some are supported by recent work in our laboratory.

### 2 Test apparatus of corrosion-wear in molten metal

As mentioned above, the corrosion-wear in molten metal is not the simple sum of corrosion and wear, so the traditional testing apparatus for corrosion and wear cannot be adopted directly for evaluating the tribo-corrosion interactions. Therefore, it is necessary to

explore the testing apparatus, especially a standardized testing apparatus, to evaluate the corrosion-wear resistance performance of materials in molten metal. Since wear can be in the forms of erosion, abrasion, sliding or fretting, the test apparatus is various.

To study the equipment including rolls and supporting bearings during the hot-dip galvanizing process, some researchers developed lots of test apparatus of corrosion-wear in molten zinc. KIM et al [12,13] prepared a pin-on-disc sliding wear test machine, as shown in Fig. 1. During test, the pin specimen was kept stationary while the circular disc rotated in argon atmosphere. Not only the wear loss and the microstructure can be examined, but also the friction coefficient can be monitored by computer terminal.

ZHANG et al [14–16] prepared another test rig, where a hollow drive shaft is supported by two large pillow blocks and the motor and shaft are inclined at approximately 30° from horizontal, as shown in Fig. 2 [16]. This special structure requires large crucible, and thus increases the cost.

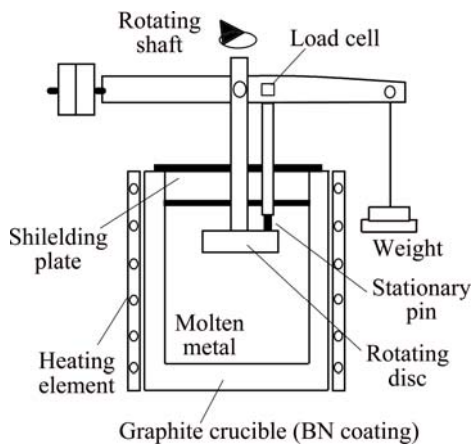


Fig. 1 Schematic representation of pin-on-disc sliding wear tester [12,13]

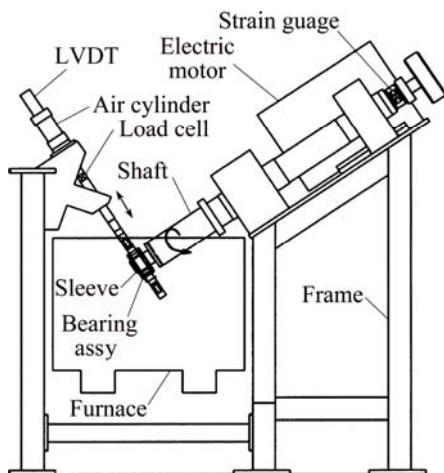


Fig. 2 Schematic of submerged bearing test rig [16]

A rotating pin test apparatus was used to investigate how flow influenced erosive-corrosive wear, as shown in Fig. 3 [17]. The effects of geometry, flow velocity, material, melt temperature, and exposure time on wear can be evaluated. However, the friction coefficient cannot be tested.

In order to learn more about issues related to friction, wear and lubrication of pieces of mechanisms of lead as a heavy liquid-metal coolant in reactor loops, BEZNOSOV et al [18] invented a high temperature test bench as shown in Fig. 4. The contact friction pair is

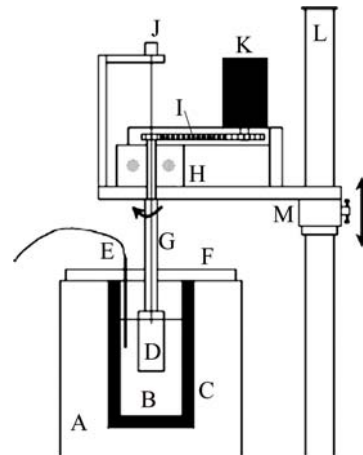


Fig. 3 Illustration of erosion-corrosion test apparatus [17]: A—Resistance furnace; B—Aluminum melt; C—Graphite crucible; D—Pin; E—Sheathed thermocouple; F—Fibrefrax insulation; G—Steel shaft; H—Water-cooled bearing housing; I—Gear and chain assembly; J—Rotation assembly; K—Motor; L—Support column; M—Control arm

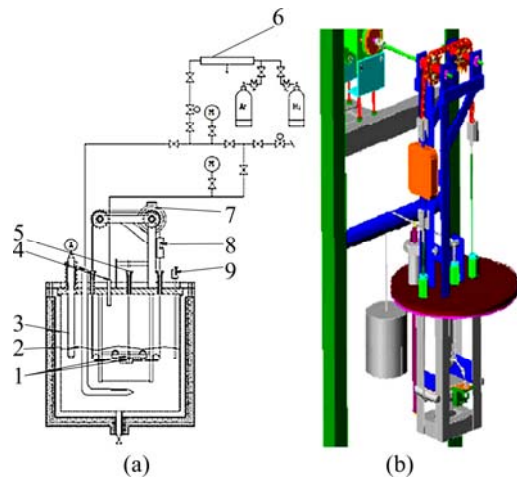
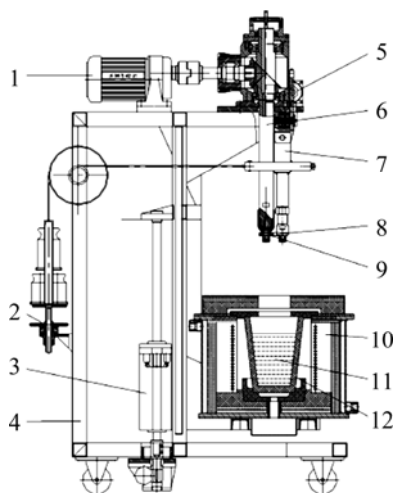


Fig. 4 Diagram of TR-2010 high temperature test bench (a) and model (b) [18]: 1—Contact friction pair under test; 2—Free surface level of heavy liquid-metal coolant (lead); 3—Oxygen thermodynamic activity sensor; 4—Gas inlet and outlet tubes; 5—Loading system; 6—Gas system manifold; 7—Motor; 8—DOU-31 dynamometer tension gage; 9—Temperature sensor

completely submerged into a lead coolant. There are two kinds of test bench. Compared with test bench TR–2010, test bench TR–2012 is optimized and upgraded, and it is designed to determine the frictional coefficient of the contact friction pairs of samples of steel in heavy liquid metal coolant at 450–550 °C.

A new test apparatus was made in our laboratory as shown in Fig. 5 [19]. The friction pair is under ring-block structure with test material being block and the ring being  $\text{Si}_3\text{N}_4$ . Since it can be lifted to make the friction pair submerged in molten aluminum, the crucible can be small and only about 3 kg pure Al will be enough. The load is applied through a wire rope, and the direction of force application is parallel to the direction of the normal stress between the friction pair, so the applied force is more accurate. Meanwhile, the friction coefficient is monitored by computer terminal. This test rig works well, and it will be helpful to explore new materials with excellent corrosion-wear resistance in molten metal.



**Fig. 5** High temperature test rig for corrosion-wear in molten metal made by SCUT [19]: 1—Electromotor; 2—Force loading system; 3—Furnace lifting device; 4—Frame; 5—Pressure sensor; 6—Rotating shaft; 7—Loading lever; 8—Cuboid specimen; 9—Annular friction pair; 10—Furnace; 11—Molten metal; 12—Crucible

Each of the test apparatus shown above has its advantage, to some extent, the corrosion-wear resistance performance of materials in molten metal can be investigated. However, there is still no standardized test apparatus in the market.

### 3 Corrosion-wear resistance performance of Fe-based materials in molten Al and its alloys

Fe-based materials are the mostly used materials for mould and crucible in aluminum industry, so lots of

researches were conducted to investigate their corrosion resistance performance in molten aluminum and its alloys. It was found that an aluminide coating was formed at the interface between a solid and molten Al. The corrosion mechanism of molten Al is essentially similar to hot-dip aluminizing, so many analyses on the interface reactions, the formations of Fe–Al intermetallics and the corresponding mechanisms can use it for reference when study the corrosion of molten Al.

#### 3.1 Corrosion resistance performance of Fe-based materials

The corrosion of Fe-based materials in molten aluminum and its alloys mainly results from the Fe-based materials wetted by molten aluminum, dissolution of Fe and the diffusion of Al towards Fe substrate. The latter one is called reaction diffusion and can form intermetallic compounds (IMCs) composed of major  $\text{Fe}_2\text{Al}_5$  ( $\eta$  phase) and minor  $\text{FeAl}_3$  ( $\theta$  phase) (shown in Fig. 6) [20], driven by the difference of chemical potentials for Fe and Al between the matrix and the melt. Corresponding morphology evolution and growth kinetics of the intermetallic layers of  $\text{Fe}_2\text{Al}_5$  and  $\text{FeAl}_3$  were established as a function of time and temperature. It was found that the growth kinetics of the  $\text{Fe}_2\text{Al}_5$  layer agrees well with a parabolic rate law expect the initial stage because the initial stage is caused by an interface control reaction at the beginning of the process, while the  $\text{FeAl}_3$  layer is governed by linear kinetics. The growth direction of  $\text{Fe}_2\text{Al}_5$  layer always grows towards Fe matrix, owing to the orthorhombic crystal structure that contains about 30% voids along the  $c$ -axis, which makes Al diffuse much more easily into the inter-diffusion front. The interface between the  $\text{Fe}_2\text{Al}_5$  and Fe substrate has a serrated or tongue morphology (as shown in Fig. 7 [20]), and thus the  $\text{Fe}_2\text{Al}_5$  phase exhibits a preferred lattice orientation (as shown in Fig. 8 [21]). The interface tends to flatten with the increase in immersion time. Because of the great difference in inter-diffusion

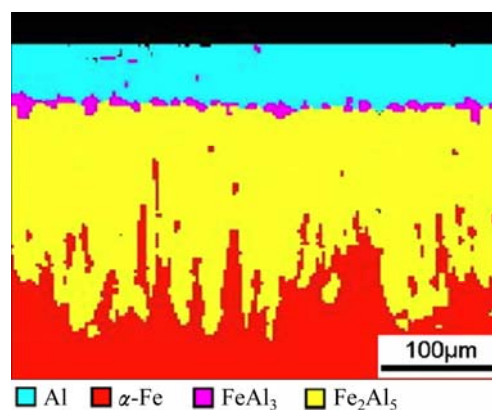


**Fig. 6** EBSD analysis showing phase distribution map of mild steel after hot-dipping [20]

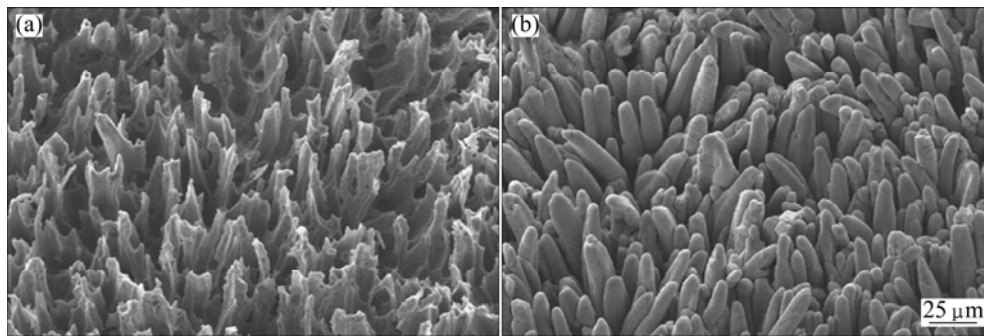


**Fig. 7** Mild steel coated by hot-dipping for 180 s, after etching, revealing Fe–Al/steel substrate interface morphology of steel substrate (a) and  $\text{Fe}_2\text{Al}_5$  (b) [20]

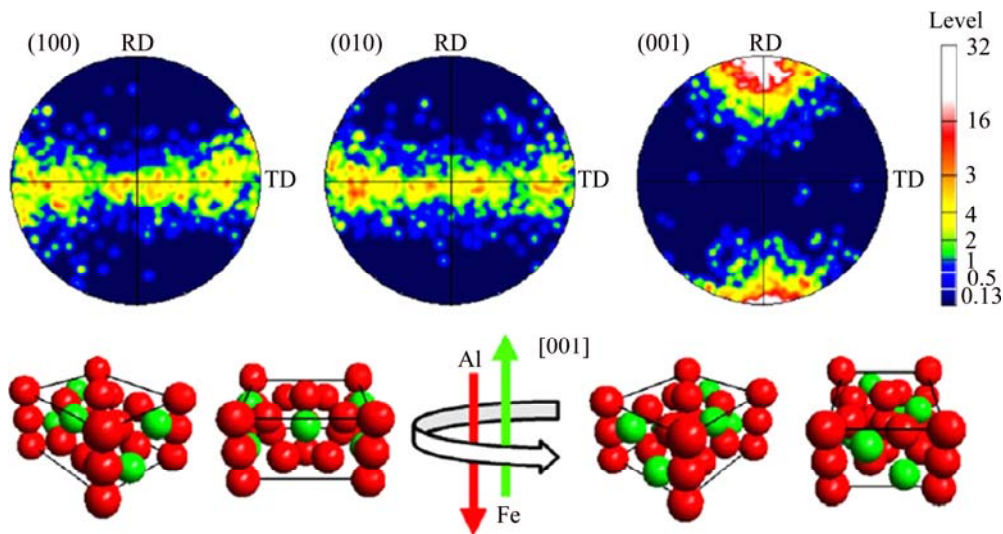


**Fig. 8** (100), (010) and (001) pole figures of  $\text{Fe}_2\text{Al}_5$  phase after diffusion in air at 750 °C for 15 min analyzed by EBSD, and schematic diagrams of orientation of  $\text{Fe}_2\text{Al}_5$  phase showing  $\text{Fe}_2\text{Al}_5$  fixed its  $c$ -axis, [001], along Al/Fe inter-diffusion direction [21]

coefficients of Fe and Al within  $\text{Fe}_2\text{Al}_5$ , voids are often generated along the interface between the aluminide layer and the matrix, which is called the Kirkendall effect. Different from the Fe–Al phase diagram, FeAl phase cannot be detected at all, while  $\text{FeAl}_2$  phase can only be in the matrix under special conditions [22–25], due to the difference of thermodynamics, nucleation and growth kinetics. The Al concentration along the coating and substrate after hot dipping is shown in Fig. 9 [26]. It is indicated that, there is not only a small concentration gradient in the  $\text{FeAl}_3$  and  $\text{Fe}_2\text{Al}_5$  layers, but also in the steel substrate below the last intermetallic layer. The diffusion gradient in the Fe–Al solid solution starts at the solubility limit of about 32.6% Al (mass fraction) and reaches the original concentration of the steel substrate after a short distance. So, the Al concentration in the sample after hot dipping is not continuous, which is a characteristic of reaction diffusion.

When dissimilar metals contact with each other at elevated temperatures, the new phases forming between them depend on three factors: 1) chemical potentials, 2) nucleation conditions at the beginning of the

inter-diffusion process, 3) mobility of the constituent elements. Based on these, there are several methods developed to retard the corrosion. Adding Al in cast iron could reduce the chemical potential differences, so the driving force would be reduced. Another way to limit the diffusion of atoms is creating some obstacles, such as graphite lamellas, eutectoid or duplex phase structure, which has been proved by many articles [8,27–29].

The morphology and growth kinetics of intermetallic compounds can also be affected by alloying elements, such as Si, Cr, Cu and C. Among these elements, Si has the greatest effect, whenever it contains in the matrix or is added in the Al bath. High silicon ductile iron was coated by hot-dipping into an Al molten bath, the coating layers consisted of three layers, in the sequence of Al, Fe–Al intermetallic and Si pile-up layers from the external topcoat to the substrate. Fe–Al–Si compounds could not be found, the Si containing in the substrate would reduce the growth rate of  $\text{Fe}_2\text{Al}_5$  [30]. The existence of Si-rich phase between the substrate and  $\text{Fe}_2\text{Al}_5$  was also found by LOU et al [8]. However, it is not clear whether the Si-rich phase is formed during hot

dipping or during the slow cooling of the samples in air. Fe–Si steels with gradient Si content were hot-dipped. INFANTE et al [31] found that the interfaces of Al/FeAl<sub>3</sub>, FeAl<sub>3</sub>/Fe<sub>2</sub>Al<sub>5</sub> and Fe<sub>2</sub>Al<sub>5</sub>/steel became smoother as Si content increased. When Si was added to the Al bath, something different happened, some Fe–Si–Al phases (such as Al<sub>7</sub>Fe<sub>2</sub>Si and Al<sub>2</sub>Fe<sub>3</sub>Si<sub>3</sub>) were formed (as shown in Fig. 10 [32]). Furthermore, as the silicon content in the aluminum bath increased, the thickness of the intermetallic layer decreased, and the intermetallic

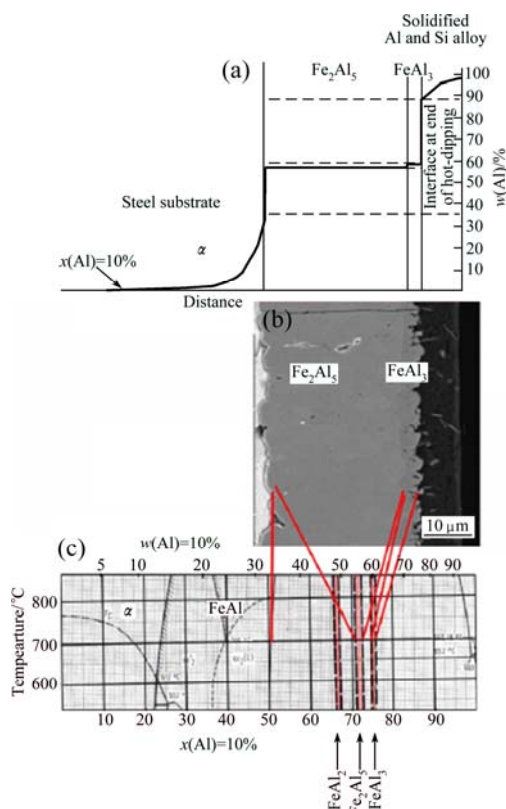


**Fig. 9** Schematic representation of Al content along coating and substrate after hot dipping (a), SEM micrograph after hot dipping (b) and section of binary Fe–Al phase diagram (c) [26]

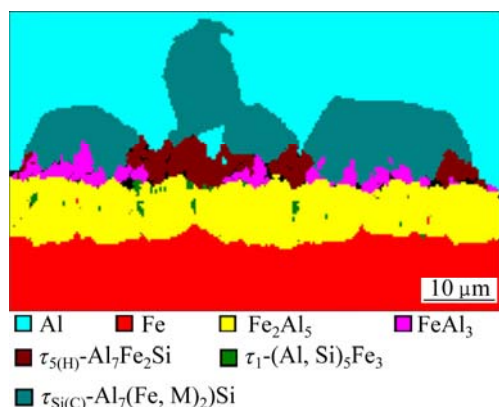


**Fig. 10** Cross-sectional EBSD phase distribution map of intermetallic layer on mild steel after hot-dipping in Al–5Si molten bath at 700 °C for 180 s [32]

layer/substrate interface became more flat. CHENG and WANG [32–36] concluded that Si added into the molten Al induced the formation of Al<sub>2</sub>Fe<sub>3</sub>Si<sub>3</sub> precipitates in the Fe<sub>2</sub>Al<sub>5</sub> layer by the serration-like steel substrate reacting with the Fe<sub>2</sub>Al<sub>5</sub> layer containing solid-solution Si. Si occupies the structural vacancies in the *c*-axis of Fe<sub>2</sub>Al<sub>5</sub>, which can impede the inter-diffusion of Fe and Al in the Fe<sub>2</sub>Al<sub>5</sub>. HOU et al [37] reported that the existence of Si decreased the activity coefficient of Al in the phase of Fe–Si–Al and prevented Al moving from molten Al to the steel substrate. YIN et al [38] concluded that Si could reduce the activation energy of Fe<sub>2</sub>Al<sub>5</sub> resulting from the lattice distortion as Si penetrated into the Fe<sub>2</sub>Al<sub>5</sub> phase by occupying the vacancy site to block facile diffusion path. The decrease of the thickness of the intermetallic layer could also be attributed to the detachment of exterior of the intermetallic layer into the Al bath. When pure Fe was hot-dipped in the Al–8.2Mg–4.8Si alloy at 750 °C for some times, TAKATA et al [39] found that the Fe<sub>2</sub>Al<sub>5</sub> phase layer grew one order of magnitude slower in the Al–Mg–Si alloy melt than that in the pure Al melt. The retarded interfacial reaction between solid Fe and liquid Al–Mg–Si alloy is ascribed to a continuous FeAl<sub>3</sub> phase layer formed in the Al–Mg–Si alloy melt, which acts as the diffusion barrier. Thus, the addition of Si and Mg into the Al melt significantly prevents the two interfacial reactions of the growth of the Fe<sub>2</sub>Al<sub>5</sub> phase layer and dissolution of Fe into the pure Al melt, and the schematic illustration is shown in Fig. 11 [39]. In addition, others contributed the effect of Si on changing the morphology of the intermetallic layer, either due to the fact that Si would reduce the preferential nucleation of aluminide crystallites on certain crystallographic planes of the substrate [26], or due to an increase in the interface energy [28]. However, there are some controversial views about the effects of Si on the reaction layers until now. For example, SPRINGER et al [40] found that the addition of Si to Al could accelerate the reaction layer growth in solid/semi-solid inter-diffusion experiments.

Another important alloy element is Cr. When the Cr–Mo steel with different Cr contents was coated by hot-dipping into molten Al–10Si bath for 180 s, besides the intermetallics mentioned above, Al<sub>7</sub>(Fe,Cr)<sub>2</sub>Si was formed, while only FeAl<sub>3</sub> and Fe<sub>2</sub>Al<sub>5</sub> were formed as the steel was immersed in pure aluminum bath, regardless of the Cr content in the steels [41–43], but the reasons were not given. When A 316L stainless steel was coated by dipping it into a molten Al–12.4Si alloy, a uniform layer of intermetallic Al<sub>12</sub>(Fe,Cr)<sub>3</sub>Si<sub>2</sub> is formed, the thickness of it is irrespective of the immersion time, and the nanomechanical properties have been studied [44–47].

It is generally known that the growth rate of the intermetallic layer is strongly dependent on many

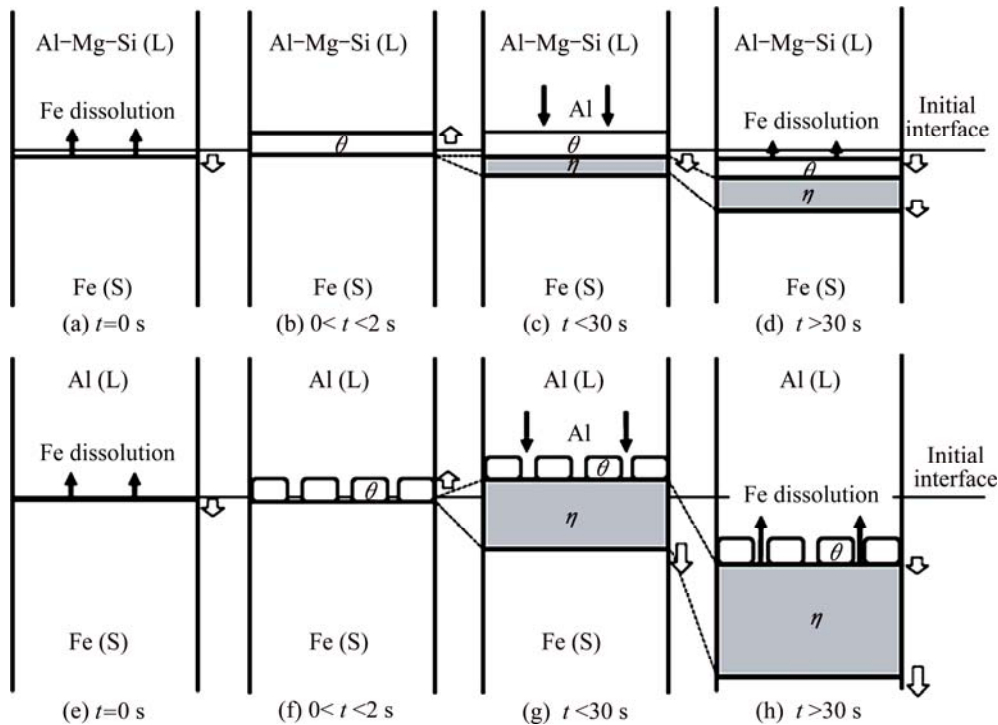


**Fig. 11** Schematic illustration of growth process of  $\eta$  and  $\theta$  phase layers during dipping Al-Mg-Si alloy (a-d) and pure Al (e-h) melts [39]

factors, including the composition of aluminizing metal, carbon content of Fe-based alloys, dipping time and the aluminizing temperature, etc. For instance, the variation of the temperature of molten aluminum and its alloys could change the relative volume fractions of the phases of ferrite, pearlite and austenite in the Fe-based substrate, and thus affect the corresponding growth rate of the intermetallic layer. The pearlite and the austenite can decrease the growth rate of the intermetallic layer, and the impeding intensity of the austenite phase is greater than the pearlite phase, whereas the ferrite phase appears to dissolve more easily [25].

### 3.2 Corrosion-wear resistance performance of Fe-based materials

The researches on corrosion-wear resistance performance of Fe-based materials in molten Al and its alloys are focused on erosion, abrasion, washout, soldering and dynamic Al liquid. The corrosion wear testing carried out by high pressure die-casting was mainly based on two mechanisms: 1) physical corrosion (dissolution, liquid-impingement erosion and solid erosion), 2) chemical corrosion. H13 steel exhibits a middle corrosion wear resistance performance (Fig. 12 [48]). HWANG et al [49] found that the dissolution of the steel substrate was under the control of diffusion mechanism by using a test similar to the test apparatus as shown in Fig. 3. YANG et al [50] investigated the corrosion of 1Cr18Ni9Ti electrode in molten Al. They found that the corrosion interface thickness in dynamic

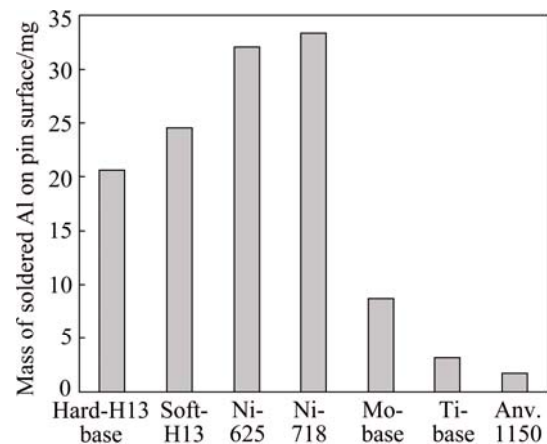


**Fig. 12** Effect of pin materials on soldering after 50 shots [48]

molten Al was much thinner than that in static molten Al owing to the scour by the dynamic flowing of molten Al, and the intermetallic layers were composed of FeAl and  $\text{Fe}_2\text{Al}_5$ , no Cr was found in the intermetallic layers, which was different from the intermetallics reported in Refs. [41–47].

In our laboratory, we have done some work by applying the test apparatus as shown in Fig. 5. Our results showed that there were more micro-cracks on the corrosion-wear surface of H13 steel than those on tungsten (W). Meanwhile, micro-ploughing appeared on both of them. To our surprise, the friction coefficient decreases significantly and remains at a low level during the testing. The average corrosion rate of tungsten in molten Al is about 1/14 that of H13 steel, the loss rate of

tungsten under corrosion-wear condition is only about 1/24 that of H13 steel, demonstrating that the corrosion-wear resistance of tungsten is much superior to that of H13 steel [51].

## 4 Corrosion-wear resistance performance of other materials

### 4.1 Refractory metals and alloys

In contrast to the non-homogeneous and dramatic reaction between Fe and liquid Al, the reaction between Co and liquid Al was homogeneous and modest. Co alloys reacted rapidly, an interfacial two-layer structure formed between Co alloys and molten Al, and Co alloys lost the thickness with a linear law with respect to immersion time. The interfacial reaction was controlled by the dissolution of the intermetallic compounds. Alloying elements such as Cr and Mo changed the solid-liquid interface structure, but had no effect on the corrosion mechanism [52–56]. When Nb was dipped into molten Al, the NbAl<sub>3</sub> intermetallic compound was formed, the corrosion mechanism was also the dissolution of Nb and spalling of Nb–Al intermetallic compounds due to thermal stresses and dispersed in the bath, the mass-loss varied linearly with time [57,58]. The intermetallic compounds between Ti–6Al–4V and Al–Si molten consisted of laminar Ti<sub>7</sub>Al<sub>5</sub>Si<sub>12</sub> phase and granular TiAl<sub>3</sub> [59]. The results shown in Fig. 13 [60] on the corrosion of 91W–6Ni–3Fe in molten Al agree with results in Fig. 12, showing that W alloys have the best corrosion-wear resistance properties, while Ni exhibits the worst properties.

However, those metallic alloys are very expensive, which will limit their extensive application in modern industry.

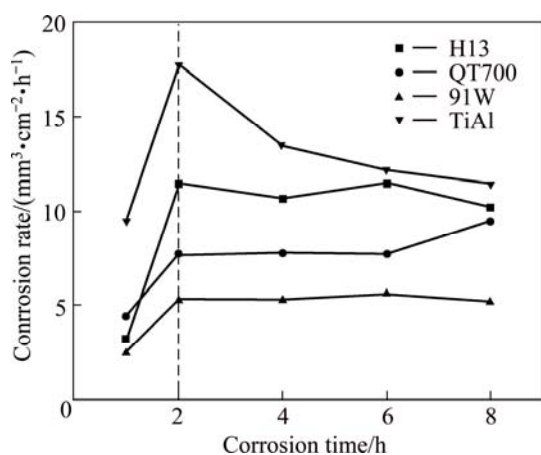


Fig. 13 Corrosion rate of different materials dipping in molten Al [60]

### 4.2 High entropy alloys

Because of unique compositions, microstructures

and adjustable properties, high-entropy alloys (HEAs) have attracted increasing attention recently. There are also some other names, such as multi-principal-elements alloys, equi-molar alloys, equi-atomic ratio alloys, substitutional alloys, and multi-component alloys [61,62]. Therefore, the potential of HEAs for use as the crucible materials for Al melts is of interest. After a FeCoNiCrMnAl HEA was prepared by vacuum induction melting, the hot dipping test was conducted. The results showed that the contact between the solid substrate and the Al melt resulted in the formation of complicated microstructure at the interface. The dissolution of the substrate alloying elements into the Al melt also caused chemical composition and phase changes in the solidified Al crust [63]. FU et al [64] investigated the corrosion behaviors of Al<sub>0.5</sub>FeNiCr and Al<sub>0.5</sub>FeNiCoCrTi<sub>0.2</sub> and found that compounds produced by corrosion reaction between molten Al and alloy elements of Al<sub>0.5</sub>FeNiCr spalled from the intermetallic layer and then dissolved into the molten Al. While, two dense intermetallic layers were formed. The ability of different elements diffusing into Al melt in the two HEAs was different, following the order of Cr→Fe→Ni (in Al<sub>0.5</sub>FeNiCr alloy) and Ni→Cr→Co→Fe→Ti (in Al<sub>0.5</sub>FeNiCoCrTi<sub>0.2</sub> alloy) from large to small size. These results may provide a theoretical basis for new corrosion-resistant materials design in molten Al.

### 4.3 Intermetallics

In recent years, increasing research interest has been seen in the development of IMCs. Intermetallics constitute a unique class of materials that have many exciting and advantageous properties in a wide variety of applications. A number of IMCs are also being developed for use in structural applications. Some examples of these materials include Ni<sub>3</sub>Al, NiAl, Fe<sub>3</sub>Si, and FeSi. Different Fe–Si IMCs were fabricated by mechanical alloying and annealing treatment, and FeSi had the best anticorrosion ability in molten Al, SiC was the next and Fe<sub>3</sub>Si was the worst [65]. However, the manufacturing process of IMCs is very complex and cost-intensive.

### 4.4 Ceramics

Ceramics including graphite, aluminosilicate refractories, AlN, Si<sub>3</sub>N<sub>4</sub>, and Al<sub>2</sub>O<sub>3</sub> are widely used for aluminum melting applications. Refractories for dealing with molten Al face severe corrosion and degradation issues due to the extremely reducing nature of molten Al. Refractory corrosion results in the recession of hot face (working surface) due to chemical reaction and molten metal penetration. Therefore, the focus of refractory development has shifted to minimize aluminum attack and subsequent molten metal penetration using

non-wetting additives such as  $\text{BaSO}_4$ ,  $\text{SrSO}_4$  and  $\text{AlPO}_4$  [66,67]. The corrosion resistance of ceramics can also be improved by decreasing the porosity and controlling their grain size to close open cracks in the molten Al [68]. The knowledge gained in this project has enabled the development of some new materials that exhibit excellent corrosion and wear resistance. One material is a castable refractory based on calcium aluminate (bonite) ( $\text{CaO}\cdot 6\text{Al}_2\text{O}_3$ ), the other material is an alumina/silicon carbide composite material (approximately 53% SiC, 35%  $\text{Al}_2\text{O}_3$ , and 12% Al or 12% Si, mass fraction). It is also an alumina–silicon carbide composite refractory containing a continuous microscopic network of interpenetrating microscopic scaled ceramic and metallic phases [69]. However, its low toughness makes ceramics hard for the fabrication of complex components, where stress-bearing is a requirement [70].

#### 4.5 Ceramics/metal composites

Ceramics/metal composites ideally combine the high hardness of ceramics with the ductility of metals, and they can sever well in the corrosion-wear environment in molten Al. The corrosion-wear resistance properties of H13 steel can be improved by a  $\text{Ti}(\text{Al},\text{O})/\text{Al}_2\text{O}_3$  composite coating. Composite coatings showed significantly lower dissolution in molten Al compared with the uncoated H13 steel [71]. RIO et al [72] produced co-continuous ceramic composites (whose acronym is C4) by reactive metal penetration, composed of NiAl and  $\text{Al}_2\text{O}_3$ . C4 composites are metal/ceramic ones consisting of two interpenetrating continuous networks. One is a metallic alloy, the other is a ceramic phase. Similar research has been also done by PAVESE et al [73–78]. These C4 have the following characteristics: high melting point, NiAl intermetallic and  $\text{Al}_2\text{O}_3$  with superior anticorrosion of molten Al, thermodynamic compatibility and close thermal expansion coefficients. So, the NiAl– $\text{Al}_2\text{O}_3$  C4 represents a potential high-temperature material. Excera Materials Group has developed a manufacturing process of a kind of co-continuous composite of alumina with about 30% NiAl, which had been used for liquid metal handling applications [79].

In our laboratory, an in-situ  $\text{Ti}_3\text{AlC}_2$  and  $\text{Al}_2\text{O}_3$  cooperatively reinforced  $\text{TiAl}_3$  composite, which was also a co-continuous ceramic–metal composite (C4), was synthesized from a mechanically milled powder mixture by using an in-situ reaction/hot pressing method. The corrosion-wear volume loss of H13 tool steel is about 133–407  $\text{mm}^3/\text{h}$ , and the synergy ratio of corrosion-wear is not less than 93.9% under the explored condition. Compared with H13 tool steel, the corrosion-wear resistance of  $\text{TiAl}_3/\text{Ti}_3\text{AlC}_2/\text{Al}_2\text{O}_3$  composite has

improved significantly. The corrosion-wear volume loss of the composite is only 0.84–7.53  $\text{mm}^3/\text{h}$ , which is dozens or even hundreds times less than that of H13 [80].

## 5 Discussion

### 5.1 Basic processes and expressions of corrosion and wear

A corrosion modeling was constructed for the homogeneous interfacial reactions of a solid metal with liquid metal, as shown in Figs. 14 [56] and 15. When the solid metal (A) contacts with the liquid metal such as aluminum (B), atoms of the solid material A dissolve and diffuse into the melt or the intermediate zone in the initial stage of interaction. This occurs on a small scale, generally as individual atoms. As the content of A at the A/B interface increases to the minimum content to form the  $\text{A}_p\text{B}_q$  phase, the nucleation of the  $\text{A}_p\text{B}_q$  is formed, then a continuous layer of IMC ( $\text{A}_p\text{B}_q$ ) is established and grows thicker with the reaction time at the solid–liquid interface (A/B interface). At the interface between solid A and IMC (interface I), B atoms that diffuse through the intermetallic layer react with A and form more IMC, driving the interface I toward the solid metal side as the solid metal is consumed. The IMC layer is not stable in liquid B and may dissolve into it through the interface between the IMC and liquid B (interface II). This process would cause interface II to move toward the solid metal side. The thickness loss of the solid A ( $\Delta X$ ) reflects the

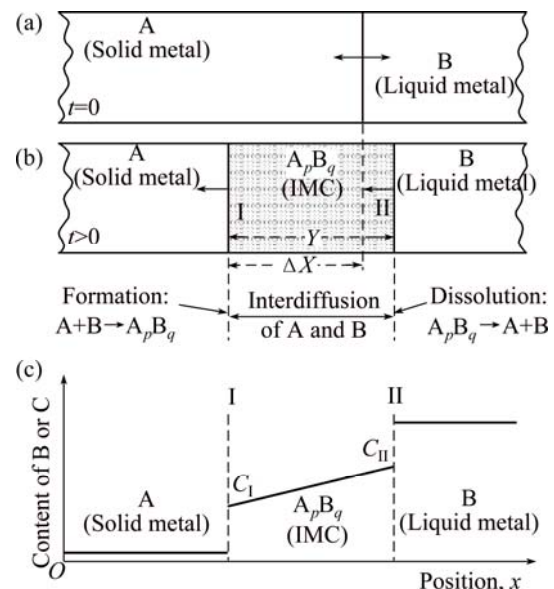


**Fig. 14** Schematic diagrams of model of interfacial reaction between solid metal A and liquid B: (a) At  $t=0$ , solid metal coming into contact with liquid Al; (b) At  $t>0$ , layer of IMC ( $\text{A}_p\text{B}_q$ ) formed at interface with thickness of  $Y$ , at this moment, solid metal losing thickness of  $\Delta X$ ; (c) Content profile of Al across interface,  $C_I$  is content of Al at interface I,  $C_{II}$  is concentration of Al at interface II [56]

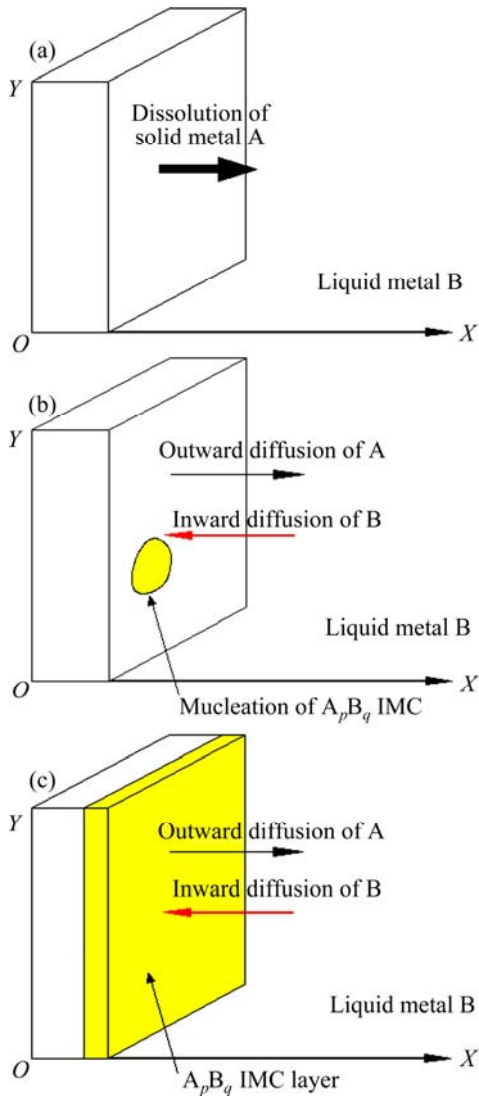


**Fig. 15** Schematic diagram showing formation of IMC: (a) Dissolution of A into B in initial stage of interaction; (b) Nucleation of IMC ( $A_pB_q$ ); (c) Establishment of continuous layer of IMC

movement of interface I, and the evolution of the thickness of the IMC ( $Y$ ) reflects the relative motion of interface I and interface II. For the narrow composition range of IMC, the inter-diffusion coefficient is considered to be independent of composition, and the concentration gradient of B in the IMC is independent of position. In this stage in the interfacial layer, the corrosion rate is controlled by inter-diffusion of the reacting species through different phases [56].

As for a homogeneous interfacial reaction, the diffusion flux normal to the interface can be expressed as Fick first law [56]:

$$J = -D \frac{dC}{dx} \quad (1)$$

where  $J$  is flux of atom B;  $D$  is the inter-diffusion

coefficient of the IMC;  $C$  is concentration of B in the IMC;  $x$  is the position along the diffusion direction, and the negative sign indicates the opposite directions of the diffusion flux and concentration gradient.

It is known that

$$\frac{dC}{dx} = \frac{C_I - C_{II}}{Y} \quad (2)$$

where  $Y$  is the thickness of the IMC, then,

$$J = D \frac{C_{II} - C_I}{Y} \quad (3)$$

At the interface I, if in a duration  $dt$  the new IMC formed has a thickness of  $dY_f$ , then  $dt$  and  $dY_f$  are related as follows:

$$JAdt = \frac{q\rho_{IMC}SdY_f}{W_{IMC}} \quad (4)$$

$$D \frac{C_{II} - C_I}{Y} Adt = \frac{q\rho_{IMC}SdY_f}{W_{IMC}} \quad (5)$$

where  $t$  is the immersion time;  $q$  is the stoichiometric coefficient of B in the IMC ( $A_pB_q$ );  $\rho_{IMC}$  is the density of the IMC;  $S$  is the area of the interface;  $Y_f$  is the thickness of the formed IMC; and  $W_{IMC}$  is the molar mass of the IMC ( $A_pB_q$ ).

Then, the formation rate of IMC can be expressed as

$$\frac{dY_f}{dt} = \frac{W_{IMC}D(C_{II} - C_I)}{q\rho_{IMC}} \frac{1}{Y} = \frac{\alpha}{Y} \quad (6)$$

where  $\alpha$  is a constant.

At interface II, the dissolution of IMC into liquid B can be described by the Nernst–Shchukarev equation [81]:

$$\frac{dc}{dt} = k \frac{S}{V} (c_s - c) = c_s [1 - \exp(-\frac{kS}{V}t)] \quad (7)$$

Or its integrated form (with initial condition  $c=0$  at  $t=0$ )

$$c = c_s [1 - \exp(-\frac{kS}{V}t)] \quad (8)$$

where  $c$  is the concentration of the dissolved solid metal in the melt,  $c_s$  is the saturated concentration of the solid metal,  $k$  is the dissolution rate constant, and  $V$  is the volume of the liquid metal.

During the time  $dt$ , a thickness  $dY_d$  of the IMC was dissolved and the concentration of metal A in liquid B increased by  $dc$ , as described by the following equation:

$$dc = \frac{\rho_{IMC}SdY_d}{W_{IMC}} \frac{p}{V} \quad (9)$$

where  $Y_d$  is the thickness of the IMC dissolved and  $p$  is the stoichiometric coefficient of metal A in IMC ( $A_pB_q$ ).

Then, the dissolution rate of the IMC can be expressed as

$$\frac{dY_d}{dt} = \frac{W_{\text{IMC}}V}{\rho_{\text{IMC}}pS} k \frac{S}{V} (c_s - c) = \frac{c_s k W_{\text{IMC}}}{\rho_{\text{IMC}}p} \exp\left(-\frac{kS}{V}t\right) \quad (10)$$

Usually,  $V$  of the molten metal is large enough, so the value of  $S/V$  is close to zero ( $S/V \rightarrow 0$ ), we have

$$\frac{dY_d}{dt} \rightarrow \frac{c_s k W_{\text{IMC}}}{\rho_{\text{IMC}}p} = \beta \quad (11)$$

where  $\beta$  is a constant.

As mentioned above, the formation and dissolution of IMC happen at the same time, so the thickness evolution of the IMC can be expressed as

$$\frac{dY}{dt} = \frac{dY_f}{dt} - \frac{dY_d}{dt} = \frac{\alpha}{Y} - \beta \quad (12)$$

For the initial condition  $Y=0$  at  $t=0$ , the solution of Eq. (12) is

$$t = \frac{\alpha}{\beta^2} \ln\left(\frac{\alpha}{\alpha - \beta Y}\right) - \frac{Y}{\beta} \quad (13)$$

If we make  $dY/dt$ , meaning that equilibrium between the formation and dissolution of the IMC has been established, then

$$Y = \frac{\alpha}{\beta} = \frac{D(C_{\text{II}} - C_1)p}{c_s k q} = Y_{\text{max}} \quad (14)$$

where  $Y_{\text{max}}$  is the maximum thickness of the IMC under these test conditions.

In theoretical model, the solid metal matrix is consumed at the same time as the formation of the IMC. During time  $dt$ , the formation of a thickness  $dY_f$  of IMC means the consumption of thickness  $d(\Delta X)$  of the matrix, as expressed by the following equations:

$$\frac{\rho_A S d(\Delta X)}{W_A} = \frac{p \rho_{\text{IMC}} S dY_f}{W_{\text{IMC}}} \quad (15)$$

$$d(\Delta X) = \frac{p \rho_{\text{IMC}} W_A}{\rho_A W_{\text{IMC}}} dY_f \quad (16)$$

where  $\rho_A$  is the density of metal A and  $W_A$  is the molar mass of metal A.

The rate of thickness loss can be written as

$$\frac{d(\Delta X)}{dt} = \frac{p \rho_{\text{IMC}} W_A}{\rho_A W_{\text{IMC}}} \frac{dY_f}{dt} = \frac{p \rho_{\text{IMC}} W_A}{\rho_A W_{\text{IMC}}} \frac{\alpha}{Y} =$$

$$\frac{p W_A D(C_{\text{II}} - C_1)}{q \rho_A} \frac{1}{Y} = \theta \quad (17)$$

where  $\theta$  is a constant.

There are two special periods when the time dependence of the thickness loss can be simply expressed. The first is at the beginning of the immersion

test, when the thickness of the IMC is so small that  $\alpha/Y \gg \beta$ . In this period, we have

$$\frac{dY}{dt} = \frac{\alpha}{Y} - \beta \approx \frac{\alpha}{Y} = \frac{dY_f}{dt} \quad (18)$$

Under the initial condition  $Y=0$  at  $t=0$ , we have

$$Y = \sqrt{2\alpha t} \quad (19)$$

Then

$$\frac{d(\Delta X)}{dt} = \frac{\theta}{Y} = \frac{p W_A}{\rho_A} \sqrt{\frac{2 \rho_{\text{IMC}} D(C_{\text{II}} - C_1)}{q W_{\text{IMC}}}} \frac{1}{\sqrt{t}} \quad (20)$$

For the initial condition  $\Delta X=0$  at  $t=0$ ,

$$\Delta X = \frac{p W_A}{\rho_A} \sqrt{\frac{2 \rho_{\text{IMC}} D(C_{\text{II}} - C_1)}{q W_{\text{IMC}}}} \sqrt{t} \quad (21)$$

It is indicated that  $\Delta X$  follows a linear relationship with  $\sqrt{t}$ . In other words, the thickness loss of the metal matrix has a parabolic relationship with the immersion time. The factor  $D(C_{\text{II}} - C_1)$  indicates that the thickness loss during this period is mainly controlled by diffusion.

The other special period is after the formation and dissolution of IMC become balanced and thickness of IMC achieves its maximum value. During this period, there exist

$$\frac{d(\Delta X)}{dt} = \frac{\theta}{Y} = \frac{W_A c_s k}{\rho_A} \quad (22)$$

$$\Delta X = \frac{W_A c_s k}{\rho_A} t + a \quad (23)$$

where  $a$  is a constant of integration.

This is the linear period of the interfacial reaction, when the rate of thickness loss is related to the dissolution process by the factors  $c_s$  and  $k$ . This relation indicates that this period is mainly controlled by dissolution.

We take Fe for example. In the stable stage, the  $\text{Fe}_2\text{Al}_5$  and  $\text{FeAl}_3$  growth kinetics are described, respectively, by the following equations [82]:

$$\frac{dx}{dt} = \frac{k_{1\text{B1}} + k_{1\text{A2}}}{x} - \frac{rg}{p} k_{0\text{B2}} \quad (24)$$

$$\frac{dy}{dt} = k_{0\text{B2}} - \frac{q}{sg} \frac{k_{1\text{A2}}}{x} \quad (25)$$

where  $x$  and  $y$  are the thicknesses of  $\text{Fe}_2\text{Al}_5$  and  $\text{FeAl}_3$ , respectively,  $s$  is the stoichiometric coefficient of IMC ( $\text{A}_r\text{B}_s$ ), and  $g$  is the molar volume ratio of  $\text{A}_p\text{B}_q$  to  $\text{A}_r\text{B}_s$ .

If A is Fe, B is Al,  $\text{A}_p\text{B}_q$  is  $\text{Fe}_2\text{Al}_5$  and  $\text{A}_r\text{B}_s$  is  $\text{FeAl}_3$ , one can interpret the various coefficients as follows:

$k_{1\text{A2}}$ : Rate constant of the  $\text{Fe}_2\text{Al}_5$  layer growth by Fe diffusion at the interface with  $\text{FeAl}_3$ :  $\text{Fe}(\text{diff}) + 5\text{Fe}_2\text{Al}_5$

$\rightarrow 3\text{Fe}_2\text{Al}_5$ .

$k_{1B1}$ : Rate constant of the  $\text{Fe}_2\text{Al}_5$  layer growth by Al diffusion at the interface with Fe:  $2\text{Fe} + 5\text{Al}(\text{diff}) \rightarrow \text{Fe}_2\text{Al}_5$ .

$k_{0B2}$ : Growth rate under conditions of reaction control of  $\text{FeAl}_3$  layer growth by Al diffusion at the interface where the following chemical reaction takes place:  $\text{Al}(\text{diff}) + \text{Fe}_2\text{Al}_5 \rightarrow 2\text{FeAl}_3$ .

Therefore,  $r=1$ ,  $s=3$ ,  $p=2$ ,  $q=5$ .  $g$  is the molar volume ratio of  $\text{Fe}_2\text{Al}_5$  to  $\text{FeAl}_3$ . The densities of the compounds are  $\rho(\text{Fe}_2\text{Al}_5)=4100 \text{ kg/m}^3$  and  $\rho(\text{FeAl}_3)=4100 \text{ kg/m}^3$ , hence, the molar volumes are  $V(\text{Fe}_2\text{Al}_5)=6 \times 10^{-5} \text{ m}^3/\text{mol}$  and  $V(\text{FeAl}_3)=3.6 \times 10^{-5} \text{ m}^3/\text{mol}$ , thus,  $g=1.7$ .

Then, Eqs. (24) and (25) become

$$\frac{dX}{dt} = \frac{k_{1B1} + k_{1A2}}{x} - 0.85k_{0B2} \quad (26)$$

$$\frac{dY}{dt} = k_{0B2} - 0.98 \frac{k_{1A2}}{x} \quad (27)$$

Since the diffusion coefficient of Al atoms in steel is approximately two orders of magnitude higher than that of Fe [83], faster diffusion of Al than Fe makes  $k_{1B1}$  much higher than  $k_{1A2}$ . This statement is also confirmed experimentally to be the perturbation of the Fe/ $\text{Fe}_2\text{Al}_5$  interface.

The wear volume of a specimen is equal to the product of the average volume of a single particle and the total number of wear debris particles generated within a sliding time,  $t$ , in steady state, which can be expressed by [84]

$$V = \frac{\pi D_1^3}{6} \tilde{N} A_a t \quad (28)$$

where  $\tilde{N}$  is the number of debris particles generated in unit time on a unit apparent of the wear surface,  $A_a$  is the apparent area of contact, and  $D_1$  is the average diameter of wear debris particles.

It is reasonable to assume that during sliding wear, a micro-crack is initiated on the wear surface and will propagate for a certain distance after each contact with an asperity from the counter surface.

When wear is added to corrosion, wear and corrosion happen at the same time, the wear surface is changed by corrosion, while the corrosion surface is changed by wear.

According to the evidences available from the literature, the most common expression for the relationship of corrosion and wear is the following model [85]:

$$V_{\text{CW}} = V_{\text{C}} + V_{\text{W}} + \Delta V_{\text{S}} = V_{\text{CC}} + V_{\text{WC}} \quad (29)$$

$$V_{\text{CC}} = V_{\text{C}} + \Delta V_{\text{C}} \quad (30)$$

$$V_{\text{WC}} = V_{\text{W}} + \Delta V_{\text{W}} \quad (31)$$

$$\Delta V_{\text{S}} = \Delta V_{\text{C}} + \Delta V_{\text{W}} \quad (32)$$

where  $V_{\text{CW}}$  is the total corrosion wear loss,  $V_{\text{C}}$  is the material loss due to corrosion without the effect of mechanical wear,  $V_{\text{W}}$  is the wear loss due to wear without corrosion,  $V_{\text{CC}}$  is the material loss due to corrosion during corrosion wear,  $V_{\text{WC}}$  is material loss due to wear during corrosion wear, and  $\Delta V_{\text{S}}$  is the synergistic effect of corrosion-induced wear ( $\Delta V_{\text{W}}$ ) and wear-induced corrosion ( $\Delta V_{\text{C}}$ ).

In most cases,  $V_{\text{C}}$  and  $V_{\text{W}}$  in Eq. (29) can be tested exactly, but how to determine  $\Delta V_{\text{S}}$  properly and correctly remains a problem. Though many studies have been carried out, until now, the tribo-corrosion synergistic effects are still not well understood.

## 5.2 Synergistic effect

### 5.2.1 Effect of wear on corrosion

The material loss due to corrosion during corrosion wear is greater than the pure corrosion without wear. The reason is as follows. Firstly, the metal surface is activated by the mechanical wear. Wear can remove or damage the intermetallic layer formed during corrosion, which makes the new surface of the substrate exposure to the molten Al, more and more wear debris particles are formed, then corrosion is speeded up. Meanwhile, wear increases internal energy of the metal surface due to the plastic, normally very severe deformation, besides stress is accompanied with wear, which is similar to stress corrosion cracking. Secondly, the process of wear has the effect of dynamic agitation.

### 5.2.2 Effect of corrosion on wear

Corrosion speeds up wear in four aspects. Firstly, corrosion increases the number of micro-crack initiation sites. The stress and deformation are not non-uniform on a wear surface on a microscopic scale. Thus, the pitting will occur rendering the micro-crack initiation and propagation, which is similar to the surface corrosion fatigue cracking. As a result, the density of active crack initiation sites on a unit apparent area of the wear surface will be higher. So, there are much more sites that are potential micro-crack initiation positions for the generation of wear debris particles on a wear surface than those in a reference environment where corrosion is prohibited. Secondly, corrosion accelerates micro-crack propagation, eventually results in the breakage of the hard intermetallic layer. The propagation of the micro-crack during the formation of wear debris particles proceeds via the debonding at the crack tip (Fig. 16). If a reactive species, A, is present at the tip, and can weaken the bonding, it will promote the propagation of the crack, thus accelerating the generation of wear debris particles. The reaction between the reactive species and the bonds

at the crack tip does not need a chemical one [84]. Thirdly, some voids are formed in the intermetallic layer during corrosion, which are mainly caused by Kirkendall effect, leading to both effects mentioned above. At last, some cracks are formed in the IMCs layer due to the thermal stress and phase transformation stress during the process of corrosion. Most of the IMCs have a high hardness, so when they spall off, they will act as wear debris particles to accelerate corrosion before dissolution.

5.2.3 Synergy ratio

The synergistic effect plays an important role in attacking many industrial facilities when they are exposed to a corrosive-wear environment. So, it is very important to understand the synergistic effects of corrosion and wear when we study the corrosion-wear resistance performance of materials in molten Al. We use synergy ratio ( $S_A$ ) to characterize the synergistic effects and define it as follows:

$$S_A = \frac{V_{CW} - (V_C + V_W)}{V_{CW}} \quad (33)$$

At most of the time,  $S_A$  is positive, but sometimes,

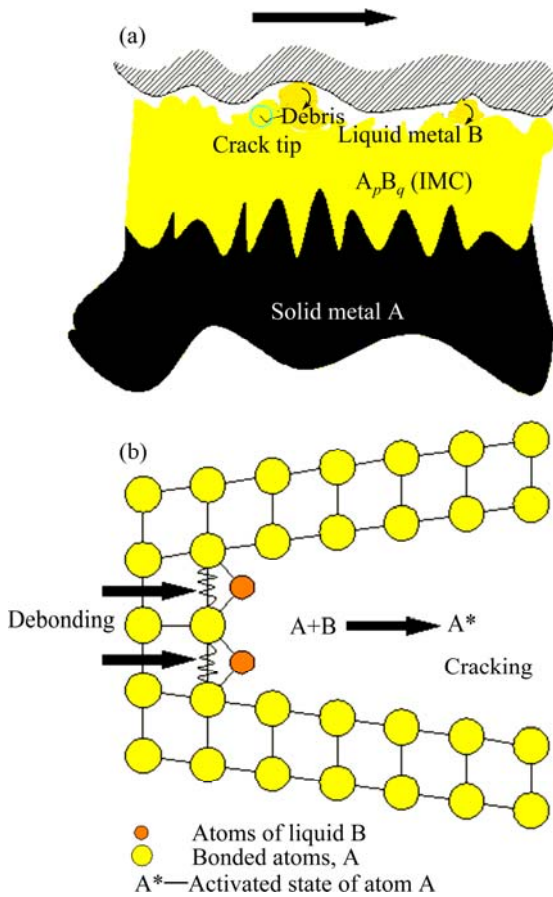


Fig. 16 Schematic diagrams showing synergistic effect of corrosion-wear in molten Al: (a) Micro-crack propagation; (b) Chemically activated reactions between reactive species A and bonds B at crack tip

$S_A$  is negative, as shown in Fig. 17 [80]. It is indicated that the corrosion-wear synergy ratio of H13 steel is much higher (>90%) than that of the co-continuous composite  $TiAl_3/Ti_3AlC_2/Al_2O_3$ . The synergy ratio is great difference under different conditions even a negative synergy ratio appears. Thus, there may be some other factors to influence the process of corrosion-wear. However, reports on these are limited.

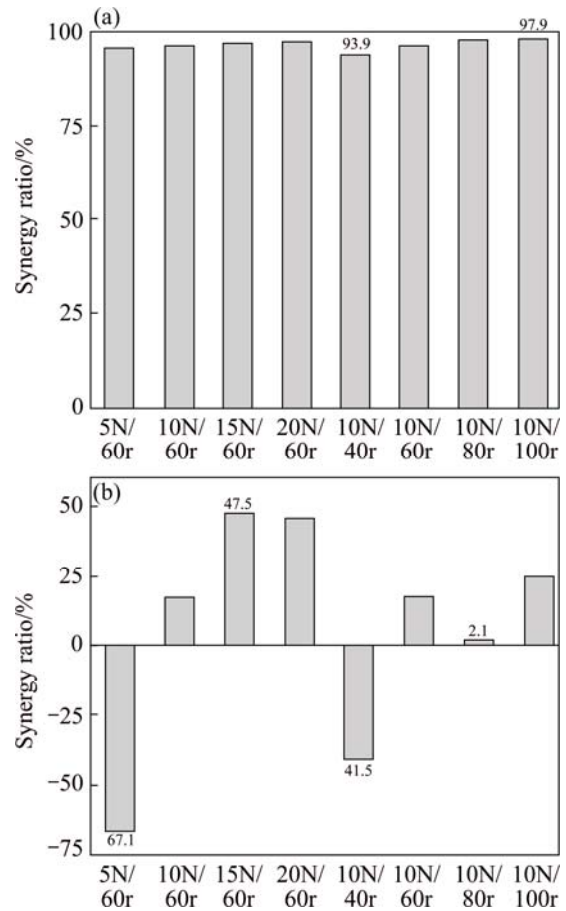


Fig. 17 Corrosion-wear synergy ratio [80]: (a) H13 steel; (b)  $TiAl_3/Ti_3AlC_2/Al_2O_3$  composite

5.3 Other effects on corrosion-wear

5.3.1 Effect of dynamic agitation due to rotating of friction

The dissolution of a solid metal into a liquid metal is described by the Nernst–Shchukarev equation as shown in Eq. (7).

When wear starts, the melt is stirred, and the dissolution rate constant,  $k$ , can be calculated by the equations below [86]:

$$k = 0.62D^{2/3} \nu^{-1/6} \omega^{1/2} \quad (S_c = \nu/D > 1000) \quad (34)$$

and

$$k = 0.55I^{-1} D^{2/3} \nu^{-1/6} \omega^{1/2} \quad (4 < S_c \leq 1000) \quad (35)$$

where  $\omega$  is the angular rotating speed of the solid metal,  $\nu$  is the kinematic viscosity of melt, and  $D$  is the

diffusion coefficient of solute across the interfacial zone and  $I=f(S_c)$ .

From the above equations, it can be indicated that the intensity of agitation affects the dissolution rate of solids in liquid. Meanwhile, the morphology of the interface between intermetallic layer and melt can be changed by agitation. Agitation can damage the protective layer or accelerate the wear by the detachment of the reaction product.

### 5.3.2 Physical effect of liquid metal

As a liquid metal, molten Al owns the characteristic of penetration or infiltration under the capillary force resulting from the wetting. The Al melt has a great infiltration capacity, and any tiny defects can be infiltrated by molten Al. The tensile stress and thermal stress of the static pressure of the Al melt will accelerate micro-crack propagation. The higher the energy of the defect is, the easier the penetration is. It is difficult to estimate either from the literature or from experiments. It is therefore difficult in this stage to make a generalized quantitative assessment of the model. However, the physical effect of liquid metal is inherent and is usually unavoidable. Another important effect of melt is lubrication. A thin molten Al film exists between the friction pairs, to some extent, it has the effects of lubrication and cooling as other lubricants.

### 5.3.3 Grain size

When solid metal A contacts with liquid melt B, atoms of B diffuse toward solid A with A diffusing toward B melt, and the  $A_pB_q$  intermetallic layer is formed between the solid A and molten B, as shown in Fig. 18. Then, B diffuses through the intermetallic layer toward the inside of A grain and reacts with A. Grain boundary is a main diffusion path. Thus, controlling the grain size will be helpful for the corrosion-wear resistance.

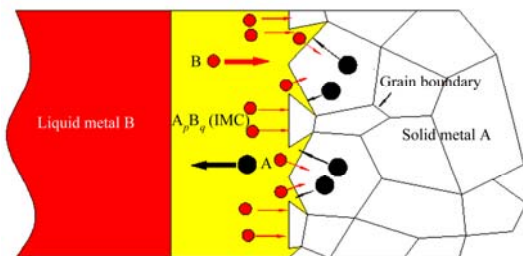


**Fig. 18** Schematic diagram showing inter-diffusion of Al and Fe

### 5.3.4 Mechanical properties at high temperature

In the process of corrosion-wear, the sample has to endure at least 700 °C for a long time, material will be softened due to the reduced mechanical properties at high temperatures. Besides, materials are exposed to liquid metal and thus liquid metal corrosion plays an

important role in the increase of the liquid metal embrittlement. Some secondary phases will precipitate when materials are exposed to high temperature for a sufficient time, which have an unignorable effect on the mechanical, wear and corrosion properties.

### 5.3.5 Volume of molten Al

The dissolution of a solid metal in molten metal is described by Eq. (7). A lot of metals will be removed from the substrate during the processing of corrosion-wear, if the molten Al becomes saturated with dissolved elements from the specimen, corrosion will be slowed.

### 5.3.6 Chemical composition of molten Al

As mentioned above, some elements (Si, Mg, Cu, etc.) have different influences on the corrosion behavior of materials in molten Al. Therefore, the chemical composition of the molten Al also plays an important role in the corrosion-wear resistance performance of materials.

## 5.4 Characteristics of corrosion-wear resistance performance

According to the research results and the discussion above, to warrant satisfactory performance in molten Al and its alloys, the materials should possess the following characteristics, in addition to necessary mechanical and thermal properties which will be helpful for the high mechanical and chemical stability properties [70].

1) Low solubility in molten Al, including the materials themselves and the intermetallic layers. Solubility is considered as the most important factor for corrosion rate. The high loss rates of nickel-based alloys are primarily due to the high solubility of nickel in liquid Al [86].

2) The intermetallic layer should be dense and be well adhered to substrate to act as a diffusion barrier, other types of obstacles such as graphite lamellas, eutectic, eutectoid or other duplex-phase structure can be helpful. Diffusion plays an important role in the process of corrosion-wear. Any measures to restrain diffusion will reduce the loss due to corrosion-wear.

3) A high hardness intermetallic layer or skeleton is required to provide protection of substrate against wear. As for the ceramics/metal composites, especially with an interpenetrating network structure, the ceramics skeleton mainly can not only bear the wear, but also protect the intermetallic layer from continuously breaking-off from the solid surface, which is similar to the action of our grabbing.

## 6 Summary

This article reviews recent progress in corrosion-wear resistance performance of materials in molten Al and its alloys. In addition, the test apparatus of corrosion-

wear in molten metal is also reviewed. The considerable volume of research on corrosion-wear of metals by molten Al and its alloys can be ascribed to the historical interest in the aluminum industry (such as casting, die-casting and hot-dip-aluminizing). Corrosion-wear is a tribological process where the total material removal results in simultaneous mechanical wear and chemical corrosion. The two material-removal mechanisms depend on each other in a complicated way, and the total material removal rate is usually not simply the sum of the corrosion rate and the wear rate measured in separate experiments. Corrosion is speeded up by wear, and wear is speeded up by corrosion. The synergism where both corrosion and wear are significantly increased by the interactions between them can significantly increase total material losses in molten aluminum environments. Therefore, the damage to materials due to the coexistence of corrosion and wear has a significant impact on economics of engineering systems both directly and indirectly in terms of material loss and associated equipment downtime for repair and replacement of corroded and worn components.

In the last decade, the corrosion-wear resistance performance of a large diversity of materials has been researched in molten Al and its alloys, including metals, such as Fe-based alloys and Co-based alloys, intermetallics, high entropy alloys, ceramics and metal/ceramic composites. Among the materials used in aluminum industry, some refractory metals such as W, Ti and Nb, and ceramics/metal composites, especially in a co-continuous structure, have excellent corrosion-wear resistance properties. However, the refractory metals such as W, Ti and Co, are very expensive, which limits the application in modern aluminum industry. Generally, a reaction layer composed of intermetallic compounds is formed at the interface of metal and molten Al, which plays an important role in the corrosion-wear resistance. The solubility, thickness, density, hardness and adhesion to substrate have a great effect on the corrosion-wear resistance performance of materials. Although the ferrous alloys like H13 steel, which are widely used in the aluminum industry, can be easily attacked by molten Al and its alloys, to some extent, the lifetime of them can be improved by alloying elements and multi-phase structure. As for the ceramics/metal composites, maybe, the co-continuous construction will make it possible.

## References

- [1] ZHANG J S, LI N. Analysis on liquid metal corrosion-oxidation interactions [J]. *Corrosion Science*, 2007, 49(11): 4154–4184.
- [2] ZHANG J S. A review of steel corrosion by liquid lead and lead-bismuth [J]. *Corrosion Science*, 2009, 51(6): 1207–1227.
- [3] HOU L F, WEI Y H, LI Y G, LIU B S, DU H Y, GUO C L. Erosion process analysis of die-casting inserts for magnesium alloy components [J]. *Engineering Failure Analysis*, 2013, 33: 457–464.
- [4] ZHANG J, HOSEMANN P, MALOY S. Models of liquid metal corrosion [J]. *Journal of Nuclear Materials*, 2010, 404(1): 82–96.
- [5] SCHEID A, SCHREIMER W H, DOLIVEIRA A S C M. Effect of temperature on the reactivity between a CoCrMoSi alloy and 55 wt% AlZn baths [J]. *Corrosion Science*, 2012, 55: 363–367.
- [6] TUNTHAWIROON P, LI Y P, TANG N, CHIBA A. Enhancement of corrosion resistance of Fe–Cr–Mo alloy to molten Al by thermal oxidation in air [J]. *Corrosion Science*, 2013, 77: 97–102.
- [7] ZHOU M, LI K, SHU D, SUN B D, WANG J. Corrosion resistance properties of enamels with high B<sub>2</sub>O<sub>3</sub>–P<sub>2</sub>O<sub>5</sub> content to molten aluminum [J]. *Materials Science and Engineering A*, 2003, 346(1–2): 116–121.
- [8] LOU D C, AKSELSEN O M, ONSOIEN M I, SOLBERG J K, BERGET J. Surface modification of steel and cast iron to improve corrosion resistance in molten aluminium [J]. *Surface & Coatings Technology*, 2006, 200(18–19): 5282–5288.
- [9] WANG D Q, SHI Z Y Z, ZOU L J L. A liquid aluminum corrosion resistance surface on steel substrate [J]. *Applied Surface Science*, 2003, 214(1–4): 304–311.
- [10] ZHANG N X, WOSIK J, FRAGNER W, SONNLEITNER R, NAUER G E. Three-dimensional analysis of the growth of intermetallics phase between solid steel and molten aluminium [J]. *Intermetallics*, 2010, 18(2): 221–225.
- [11] PANAGOPOULOS C N, GEORGIU E P, MARKOPOULOS C. Corrosion and wear of zinc in various based environments [J]. *Corrosion Science*, 2013, 70: 62–67.
- [12] SOOG J H, KIM H J. Sliding wear performance of cobalt-based alloys in molten-Al-added zinc bath [J]. *Wear*, 1997, 210(1–2): 291–298.
- [13] KIM H J, YOON B H, LEE C H. Sliding wear performance in molten Zn–Al bath of cobalt-based overlayers produced by plasma-transferred arc weld-surfacing [J]. *Wear*, 2003, 254(5–6): 408–414.
- [14] ZHANG K, BATTISTON L. Friction and wear characterization of some cobalt- and iron-based superalloys in zinc alloy baths [J]. *Wear*, 2002, 252(3–4): 332–344.
- [15] ZHANG K. Wear of cobalt-based alloys sliding in molten zinc [J]. *Wear*, 2003, 255(1–6): 545–555.
- [16] ZHANG K. Effects of test conditions on the tribological behavior of a journal bearing in molten zinc [J]. *Wear*, 2005, 259(7–12): 1248–1253.
- [17] MILLER A E, MAIJER D M. Investigation of erosive-corrosive wear in the low pressure die casting of aluminum A356 [J]. *Materials Science and Engineering A*, 2006, 435–436: 100–111.
- [18] BEZNOSOV A V, NOVOZHILOVA O O, SHUMILKOV A I, LVOV A V, VOKOVA T A, MAKHOV K A. Tribotechnology problems of lead coolant in innovative fast reactors [J]. *Nuclear Engineering and Design*, 2013, 265: 675–681.
- [19] WU Jing. The screening experiments of corrosion-wear resistant metal materials in molten aluminum and device development [D]. Guangzhou: South China University of Technology, 2012. (in Chinese)
- [20] CHENG W J, WANG C J. Growth of intermetallic layer in the aluminide mild steel during hot-dipping [J]. *Surface & Coatings Technology*, 2009, 204(6–7): 824–828.
- [21] CHENG W J, WANG C J. Study of microstructure and phase evolution of hot-dipped aluminide mild steel during high-temperature

- diffusion using electron backscatter diffraction [J]. *Applied Surface Science*, 2011, 257(10): 4663–4668.
- [22] BALLOY D, TISSIER J C, GIORGI M L, BRIANT M. Corrosion mechanisms of steel and cast iron by molten aluminum [J]. *Metallurgical and Materials Transactions A*, 2010, 41(9): 2366–2376.
- [23] GASIOR W R, DEBSKI A, MOSER Z. Formation enthalpy of intermetallic phases from Al-Fe system measured with solution calorimetric method [J]. *Intermetallics*, 2012, 24: 99–105.
- [24] PAVLYUCHKOV D, PRZEPIOZYNSKI B, KOWALSKI, VELIKANOVA T Y, GRUSHKO B. Al-Cr-Fe phase diagram: Isothermal sections in the region above 50 at% Al [J]. *CALPHAD: Computer Coupling of Phase Diagrams and Thermochemistry*, 2014, 45: 194–203.
- [25] YOUSAF M, IQBAL J, AJMAL M. Variables affecting growth and morphology of the intermetallic layer (Fe<sub>2</sub>Al<sub>5</sub>) [J]. *Materials Characterization*, 2011, 62(5): 517–525.
- [26] DANZO I I, HOUBAERT Y, VERBEKEN K. Diffusion driven columnar grain growth induced in an Al-Si-coated steel substrate [J]. *Surface & Coatings Technology*, 2014, 251: 15–20.
- [27] KIM J H, KIM S Y, KANG C Y. Effect of phase difference on growth kinetic of alloy layer in aluminized and diffusion-treated 12% Cr heating resistant steels [J]. *Surface & Coatings Technology*, 2014, 240: 387–392.
- [28] AWAN G H, HASAN F U. The morphology of coating/substrate interface in hot-dip-aluminized steels [J]. *Materials Science and Engineering A*, 2008, 472(1–2): 157–165.
- [29] ZHANG X M, LI X M, CHEN W P. Interfacial reactions of duplex stainless steels with molten aluminum [J]. *Surface and Interface Analysis*, 2015, 47(6): 648–656.
- [30] LIN M B, WANG C J. Microstructure and high temperature oxidation behavior of hot-dip aluminized coating on high silicon ductile iron [J]. *Surface & Coatings Technology*, 2010, 205(5): 1220–1224.
- [31] INFANTE DANZO I, VERBEKEN K, HOUBAERT Y. Microstructure of hot dip coated Fe-Si steels [J]. *Thin Solid Films*, 2011, 520(5): 1638–1644.
- [32] CHENG W J, WANG C J. Effect of silicon on the formation of intermetallic phase in aluminide coating on mild steel [J]. *Intermetallics*, 2011, 19(10): 1455–1460.
- [33] CHENG W J, WANG C J. Observation of high-temperature phase transformation in the Si-modified aluminide coating on mild steel using EBSD [J]. *Materials Characterization*, 2010, 61(4): 467–473.
- [34] CHENG W J, WANG C J. Microstructural evolution of intermetallic layer in hot-dipped aluminide mild steel with silicon addition [J]. *Surface & Coatings Technology*, 2011, 205(19): 4726–4731.
- [35] CHENG W J, WANG C J. Study of microstructure and phase evolution of hot-dipped aluminide mild steel during high-temperature diffusion using electron backscatter diffraction [J]. *Applied Surface Science*, 2011, 257(10): 4663–4668.
- [36] CHENG W J, WANG C J. High-temperature oxidation behavior of hot-dipped aluminide mild steel with various silicon contents [J]. *Applied Surface Science*, 2013, 274: 258–265.
- [37] HOU X X, YANG H, ZHAO Y, PAN F Z. Effect of Si on the interaction between die casting die and aluminum alloy [J]. *Materials Letters*, 2004, 58(27–28): 3424–3427.
- [38] YIN Fu-chen, ZHAO Man-xiu, LIU Yong-xiong, HAN Wei, LI Zhi. Effect of Si on growth kinetics of intermetallic compounds during reaction between solid iron and molten aluminum [J]. *Transactions of Nonferrous Metals Society of China*, 2013, 23(2): 556–561.
- [39] TAKATA N, NISHIMOTO M, KOBAYASHI S, TAKEYAMA M. Morphology and formation of Fe-Al intermetallic layers on iron hot-dipped in Al-Mg-Si alloy melt [J]. *Intermetallics*, 2014, 54: 136–142.
- [40] SPRINGER H, KOSTKA, PAYTON E J, RAABE D, KAYSSER-PYZALLA A, EGGELER G. On the formation and growth of intermetallic phases during interdiffusion between low-carbon steel and aluminum alloys [J]. *Acta Materialia*, 2011, 59(4): 1586–1600.
- [41] CHENG W J, WANG C J. EBSD study of crystallographic identification of Fe-Al-Si intermetallic phases in Al-Si coating on Cr-Mo steel [J]. *Applied Surface Science*, 2011, 257(10): 4637–4642.
- [42] CHENG W J, WANG C J. EBSD characterization of high-temperature phase transformations in an Al-Si coating on Cr-Mo steel [J]. *Materials Characterization*, 2012, 64: 15–20.
- [43] CHENG W J, WANG C J. Effect of chromium on the formation of intermetallic phase in hot-dipped aluminide Cr-Mo steels [J]. *Applied Surface Science*, 2013, 277: 139–145.
- [44] FRUTOS E, GONZALEZ-CARRASCO J L, CAPDEVILA C, JIMENEZ J A, HOUBAERT Y. Development of hard intermetallic coatings on austenitic stainless steel by hot dipping in an Al-Si alloy [J]. *Surface & Coatings Technology*, 2009, 203(19): 2916–2920.
- [45] FRUTOS E, MARTINEZ-MORILLAS R, GONZALEZ-CARRASCO J L, VILABOAN. Nanomechanical properties of novel intermetallic coatings developed on austenitic stainless steels by siliconisation in liquid phase [J]. *Intermetallics*, 2011, 19(3): 260–266.
- [46] FRUTOS E, CUEVAS A, GONZALEZ-CARRASCO J L, MARTIN F. Characterization of the elastic-plastic behavior of intermetallic coatings growth on medical stainless steel by instrumented ultramicroindentation [J]. *Journal of the Mechanical Behavior of Biomedical Materials*, 2012, 16: 1–8.
- [47] FRUTOS E, GONZALEZ-CARRASCO J L. A method to assess the fracture toughness of intermetallic coatings by ultramicroindentation techniques: Applicability to coated medical stainless steel [J]. *Acta Materialia*, 2013, 61(6): 1886–1894.
- [48] ZHU Y L, SCHWAR D, WALLACE J F, BIRCEANU S. Evaluation of soldering, washout and thermal fatigue resistance of advanced metal materials for aluminum die-casting dies [J]. *Materials Science and Engineering A*, 2004, 379(1–2): 420–431.
- [49] HWANG S H, SONG J H, KIM Y S. Effects of carbon content of carbon steel on its dissolution into a molten aluminum alloy [J]. *Materials Science and Engineering A*, 2005, 390(1–2): 437–443.
- [50] YANG R F, ZHANG P, WU J H. The corrosion mechanism of a stainless electrode in the dynamic melting of Al at high temperature [J]. *Materials Science and Engineering A*, 2009, 499(1–2): 134–137.
- [51] CHEN Wei-ping, FANG Si-cong, ZENG Yong, WU Jing, LUO Hong-feng. Corrosion-wear resistant performance and mechanisms of tungsten and H13 steel in molten aluminum [J]. *The Chinese Journal of Nonferrous Metals*, 2013, 23(11): 3127–3134. (in Chinese)
- [52] TANG N, LI Y P, KURORU S, MATSUMOTO H, KOIZUMI Y, CHIBA A. Interfacial reactions between molten Al and a Co-Cr-Mo alloy with and without oxidation treatment [J]. *Corrosion Science*, 2011, 53(12): 4324–4326.
- [53] TANG N, LI Y P, KURORU S, KOIZUMI Y, MATSUMOTO H, CHIBA A. Interfacial reactions of solid Co and solid Fe with liquid Al [J]. *Corrosion Science*, 2012, 60: 32–37.

- [54] TANG N, LI Y P, KURORU S, KOIZUMI Y, KUROSU S, CHIBA A. Interfacial reaction between Co–Cr–Mo alloy and liquid Al [J]. *Corrosion Science*, 2013, 75: 262–268.
- [55] LI Y P, TANG N, TUNTHAWIROON P, KOZUMI Y, CHIBA A. Characterisation of oxide films formed on Co–29Cr–6Mo alloy used in die-casting moulds for aluminium [J]. *Corrosion Science*, 2013, 73: 72–79.
- [56] TANG N, LI Y P, KOZUMI Y, KUROSU S, CHIBA A. Experimental and theoretical research on interfacial reaction of solid Co with liquid Al [J]. *Corrosion Science*, 2013, 73: 54–61.
- [57] ROBIN A, SANDIM H R Z. Degradation behavior of niobium in molten aluminum [J]. *International Journal of Refractory Metals & Hard Materials*, 2002, 20(3): 221–225.
- [58] KOMAROV S, KUZNETSOV D. Erosion resistance and performance characteristics of niobium ultrasonic sonotrodes in molten aluminum [J]. *International Journal of Refractory Metals & Hard Materials*, 2012, 35: 76–83.
- [59] CHEN X G, YAN J C, GAO F, WEI J H, XU Z W, FAN G H. Interaction behaviors at the interface between liquid Al–Si and solid Ti–6Al–4V in ultrasonic-assisted brazing in air [J]. *Ultrasonics Sonochemistry*, 2013, 20(1): 144–154.
- [60] XIAO Hua-qiang, CHEN Wei-ping, LIU Zhe. Corrosion resistance of 91W–6Ni–3Fe refractory, TiAl compound and iron based alloys in molten aluminum [J]. *Transactions of Nonferrous Metals Society of China*, 2012, 22(9): 2320–2326.
- [61] ZHANG Y, ZUO T T, TANG Z, GAO M C, DAHMEN K A, LIAW P K, LU Z P. Microstructures and properties of high-entropy alloys [J]. *Progress in Materials Science*, 2014, 61: 1–93.
- [62] LIU C M, WANG H M, ZHANG S Q, TANG H B, ZHANG A L. Microstructure and oxidation behavior of new refractory high entropy alloys [J]. *Journal of Alloys and Compounds*, 2014, 583: 162–169.
- [63] YANG H H, TSAI W T, KUO J C, YANG C C. Solid/liquid interaction between a multicomponent FeCrNiCoMnAl high entropy alloy and molten aluminum [J]. *Journal of Alloys and Compounds*, 2011, 509(32): 8176–8182.
- [64] CHEN Wei-ping, FU Zhi-qiang, FANG Si-cong, XIAO Hua-qiang, ZHU De-zhi. Corrosion behaviors of  $Al_{0.5}FeNiCr$  and  $Al_{0.5}FeNiCrCoTi_{0.25}$  alloys in molten aluminum [J]. *China Sciencepaper*, 2013, 8(2): 166–174. (in Chinese)
- [65] GENG Gang-qiang, GUAN Lei, LI Ning, CUI Jing-na. Anticorrosion research of Fe–Si intermetallics in molten aluminum [J]. *Hot Working Technology*, 2005, 35(12): 14–16. (in Chinese)
- [66] IBARRA CASTRO M N, ALMANZA ROBLES J M, CORTES HERNANDEZ D A, ESCOBEDO BOCARDO J C, TORRES TORRES J. The effect of  $SrSO_4$  and  $BaSO_4$  on the corrosion and wetting by molten aluminum alloys of mullite ceramics [J]. *Ceramics International*, 2010, 36(4): 1205–1210.
- [67] ADABIFIROOZJAEI E, KOSHY P, SORRELL C C. Effects of  $AlPO_4$  addition on the corrosion resistance of andalusite-based low-cement castables with molten Al-alloy [J]. *Journal of the European Ceramic Society*, 2013, 33(6): 1067–1075.
- [68] TANKA M, KASHIWAGI K, KAWASHIMA N, KITAOKA S, SAKURADA O, OHYA Y. Effect of grain boundary cracks on the corrosion behavior of aluminium titanate ceramics in a molten aluminium alloy [J]. *Corrosion Science*, 2012, 54: 90–96.
- [69] HEMRICK J G, HEADRICK W L, PETERS K M. Development and application of refractory materials for molten aluminum applications [J]. *International Journal of Applied Ceramic Technology*, 2008, 5(3): 265–277.
- [70] YAN M, FAN Z. Review: Durability of materials in molten aluminum alloys [J]. *Journal of Materials Science*, 2001, 36(2): 285–295.
- [71] SALMAN A, GABBITAS B L, CAO P, ZHANG D L. The performance of thermally sprayed titanium based composite coatings in molten aluminium [J]. *Surface & Coatings Technology*, 2011, 205(21–22): 5000–5008.
- [72] RIO E D, NASH J M, WILLIAMS J C, BRESLIN M C, DAEHN G S. Co-continuous composites for high-temperature application [J]. *Materials Science and Engineering A*, 2007, 463(1–2): 115–121.
- [73] PAVESE M, FINO P, VALLE M, BADINI C. Preparation of C4 ceramic/metal composites by reactive metal penetration of commercial ceramics [J]. *Composites Science and Technology*, 2006, 66(2): 350–356.
- [74] PAVESE M, FINO P, UGUES D, BADINI C. High cycle fatigue study of metal-ceramic co-continuous composites [J]. *Scripta Materialia*, 2006, 55(12): 1135–1138.
- [75] PAVESE M, VALLE M, BADINI C. Effect of porosity of cordierite performs on microstructure and mechanical strength of co-continuous ceramic composites [J]. *Journal of the European Ceramic Society*, 2007, 27(1): 131–141.
- [76] MANFREDI D, PAVESE M, BIAMINO S, FINO P, BADINI C. NiAl(Si)/ $Al_2O_3$  co-continuous composites by double reactive metal penetration into silica performs [J]. *Intermetallics*, 2008, 16(4): 580–583.
- [77] MANFREDI D, PAVESE M, BIAMINO S, FINO P, BADINI C. Preparation and properties of NiAl(Si)/ $Al_2O_3$  co-continuous composites by double reactive metal penetration [J]. *Composites Science and Technology*, 2009, 69(11–12): 1777–1782.
- [78] MANFREDI D, PAVESE M, BIAMINO S, ANTONINI A, FINO P, BADINI C. Microstructure and mechanical properties of co-continuous metal/ceramic composites obtained from reactive metal penetration of commercial aluminium alloys into cordierite [J]. *Composites: Part A*, 2010, 41(5): 639–645.
- [79] DAEHN G S, BRELIN M C. Co-continuous composite materials for friction and braking applications [J]. *JOM*, 2006, 58(11): 87–91.
- [80] XIAO Hua-qiang. Study on fabrication and corrosion-wear resistance in molten aluminum of  $TiAl_3/Ti_3AlC_2/Al_2O_3$  composite [D]. Guangzhou: South China University of Technology, 2013. (in Chinese)
- [81] YAN M, FAN Z. The erosion of H21 tool steel in molten A380 alloy [J]. *Journal of Materials Science*, 2000, 35(7): 1661–1667.
- [82] BOUAYAD A, GEROMETTA C, BELKEBIR A, AMBARI A. Kinetic interactions between solid iron and molten aluminum [J]. *Materials Science and Engineering A*, 2003, 363(1–2): 53–61.
- [83] SHI Z M, CAO J B, HAN F S. Preparation and characterization of Fe–Al intermetallic layer on the surface of T91 heat-resistant steel [J]. *Journal of Nuclear Materials*, 2014, 447(1–3): 77–81.
- [84] JIANG J, STACK M M, NEVILLE A. Modelling the tribo-corrosion interaction in aqueous sliding conditions [J]. *Tribology International*, 2002, 35(10): 669–679.
- [85] BI Q L, LIU W M, MA J Q, YANG J, PU Y P, XUE Q J. Tribocorrosion behavior of Ni–17.5Si–29.3Cr alloy in sulfuric acid solution [J]. *Tribology International*, 2009, 42(7): 1081–1087.
- [86] YAN M, FAN Z, BEVIS M J. The erosion behavior of Inconel 718 in molten A380 alloy [J]. *Scripta Materialia*, 1999, 40(11): 1255–1261.

## 耐铝及其合金熔体腐蚀磨损材料的研究进展

张先满, 陈维平

华南理工大学 广东省金属新材料制备与成形重点实验室, 广州 510640

**摘要:** 铝及其合金熔体引起的腐蚀磨损导致材料失效是铝工业中一个非常普遍的难题。综述包括铁合金及陶瓷等材料在铝液中的腐蚀磨损行为及在液态金属中的腐蚀-磨损试验设备。在阐述单一的液态金属腐蚀和磨损机理的基础上, 分析腐蚀磨损的协同效应。综合讨论由于摩擦副旋转导致的铝液动态搅拌、液态铝物理性质以及晶粒尺寸等因素对铝液腐蚀-磨损性能的影响。最后, 总结耐铝液腐蚀磨损材料应该具备的基本特征。根据本课题组已有研究成果, 特别是  $\text{TiAl}_3/\text{Ti}_3\text{AlC}_2/\text{Al}_2\text{O}_3$  这种金属/陶瓷复合材料的优异耐铝液腐蚀磨损性能, 展望具有连续相互穿插结构陶瓷/金属复合材料在铝液腐蚀磨损环境中的应用前景。

**关键词:** 铝熔体; 铝合金; 腐蚀; 磨损; 协同效应; 金属间化合物

(Edited by Wei-ping CHEN)